Research on Multi-Point Connection of Under-Chassis Equipment Suspension System in High-Speed Trains

Yu SUN (1410745@tongji.edu.cn)
Institute of Rail Transit https://orcid.org/0000-0002-3023-4911
Jinsong Zhou
Tongji University
Dao Gong
Tongji University
Yuanjin Ji
Tongji University
Taiwen You
Tongji University
Jiangxue Chen
Tongji University
Qiushi Wang
Tongji University
Tengfei Wang
Tongji University

Original Article

Keywords: High-speed trains, Under-chassis equipment, Multi-point connection, Dynamic vibration absorber, Kinetic energy decoupling degree.

Posted Date: July 20th, 2021

DOI: https://doi.org/10.21203/rs.3.rs-716784/v1

Version of Record: A version of this preprint was published at AIP Advances on December 1st, 2021. See the published version at https://doi.org/10.1063/5.0076803.

Research on Multi-Point Connection of Under-Chassis Equipment Suspension System in High-Speed Trains

Yu Sun[a,b,*], Jinsong Zhou[b], Dao Gong[b], Yuanjin Ji[a,b], Taiwen You[b], Jiangxue Chen[b], Qiushi Wang[b], Tengfei Wang[b]

[a] *Postdoctoral Station of Mechanical Engineering, Tongji University, Shanghai 201804, PR China*

[b] *Institute of Rail Transit, Tongji University, Shanghai 201804, PR China*

Abstract: A power dispersive high-speed electric multiple-unit (EMU) train requires the installation of traction equipment under the carbody. As the speed of high-speed trains increases, the demand for traction power is increasing, and the weight and size of the equipment have increased accordingly. To adapt to the research and development of higher-speed EMU trains, this research proposes the use of a multi-point connection scheme for installing the under-chassis equipment. First, the static deflection and supporting reaction force of each hanging point are obtained based on static analysis, and it is found that increasing the number of connection points is beneficial for reducing the static stiffness requirement of each rubber element. Then, an energy decoupling degree is introduced, and an optimisation design method for the hanging point stiffness is proposed based on the energy decoupling degree and optimal vertical suspension frequency. Finally, a rigid-flexible coupling dynamics simulation model is established to analyse the vibration characteristics of the carbody and equipment after decoupling and optimisation of the multi-point suspension schemes. The research results show that after the decoupling optimisation, the vibration amplitude in the middle of the carbody is effectively reduced, and the ride quality of the carbody is improved. The difference in the number of hanging points has little effect on the vibration performance of the carbody, but increasing the number of hanging points is beneficial for reducing the dynamic supporting reaction forces of the hanging components, thereby reducing the dynamic stress of the rubber elements, and improving the fatigue resistance.

Keywords: High-speed trains; Under-chassis equipment; Multi-point connection; Dynamic vibration absorber; Kinetic energy decoupling degree.

1 Introduction

Power decentralisation technology is widely used in high-speed electric multiple unit (EMU) trains. High-speed trains with decentralisation technology can take full advantage of the wheel-track adhesive force, and effectively reduce the dynamic wheel-track interaction force. As there is no locomotive at which to place the traction equipment, many under-chassis equipment (UCE) elements need to be installed under the carbody, such as traction converters and air compressors. Some of this equipment weighs several tons, and some elements have excitation sources. If the installation method is improper, the vibration of the equipment may be transmitted to the carbody, resulting in severe adverse effects on the local and overall vibration performance of the speed-train

* Corresponding author.
E-mail address: 1410745@tongji.edu.cn

carbody.

An effective installation method is to use rubber elastic elements to isolate the vibrations from the equipment from the carbody. Sun[1] proposed a high-static-low-dynamic-stiffness mount for connecting the UCE and the carbody, which could effectively isolate the self-excitation of the air compressor from the carbody and enhance the ride quality of the high-speed train. Gong[2] studied the influences of UCE suspension system parameters on the first-order vertical bending frequency of a high-speed EMU train carbody, and designed parameters for the UCE suspension system based on mode-matching principle. Chen[3] proposed an approach for designing the suspension parameters for UCE elements, based on using a multi-objective analytical target cascading optimisation algorithm to suppress the vibration of the carbody and UCE. Wang[4] studied the effect of a dynamic imbalance in the rotational equipment on a carbody, and proposed that the use of elastic suspension for such equipment can isolate the vibration transmissions from the carbody, and that the dynamic imbalance should be considered to optimise reasonable suspension parameters.

In addition, many scholars have proposed installing UCE based on the theory of a dynamic vibration absorber (DVA)[5–7]. Shi[8] modelled a carbody as an Euler-Bernoulli beam with UCE mounted on a chassis regarded as a DVA to reduce the flexible vibration of the carbody, and proposed that the heavy equipment should be mounted to the carbody centre as close as possible to obtain a significant vibration reduction performance. Huang[9] verified that the flexible vibration of a carbody can be effectively suppressed by using the UCE as a DVA, based on roller rig tests. Gong[10] proposed a method of multi-mode vibration control for a carbody based on using multiple pieces of UCE as DVAs. An equivalent mass identification method was used to determine the equivalent mass of the target modes at the UCE installation positions. The natural frequencies and damping ratios of the lateral and vertical vibrations were designed based on the theory of the DVA. The simulation results showed that the method could significantly reduce the multi-mode vibration of the carbody, and considerably improve the ride quality in terms of the lateral and vertical vibrations of the carbody. Xia[11] studied the suspension problem of equipment with eccentricity. The vertical suspension frequency of the equipment was designed according to the principle of a DVA, and a decoupling method was adopted to ensure that the eccentric equipment could effectively play the role of the DVA.

Previous research has widely recognised the use of rubber components for elastically installing UCE, and some technologies have been applied in practice. Most of the previous studies installed the equipment based on using four hanging points. However, with further increases in the operating speeds of high-speed EMU trains, the demand for traction power is increasing, and the weight and size of the equipment under the carbody are also increasing. If the number of hanging points does not increase, the stiffness requirements of each hanging rubber element need to be increased. However, the stiffness of rubber components cannot be increased indefinitely, owing to industrial manufacturing constraints. Compared with increasing the stiffness rubber elements, increasing the number of hanging points so that the hanging system has a better load-bearing capacity could be a more practical solution.

In this study, a multi-point hanging method was proposed for connecting heavy and large eccentric equipment with a carbody. The rest of this paper is organised as follows. In Section 2, the location layout is introduced, and the static deflection and supporting reaction force of the equipment with a multi-point connection are studied. In Section 3, an optimisation method is proposed for the energy decoupling degree of the UCE. In Sections 4 and 5, a rigid-flexible coupled

vehicle dynamics model is established to analyse the carbody vibration and ride quality before and after decoupling optimisations of different multi-point connection schemes under operating conditions. The conclusions are summarised in Section 6.

2 Establishment of multi-point connection model of under-chassis equipment (UCE)

The under-chassis equipment investigated in this study was a traction converter; its mass, inertia, and size parameters are listed in Tab. 1. The eccentric distance in the x -and y-directions referred to the distance between the centre of gravity and geometric centre. The equipment was installed in the middle of the carbody, as this approach is beneficial for suppressing the vibration of the carbody[8].

Tab. 1. Parameters of the equipment

Parameter	Symbol	Value	Unit
Mass	M_e	8000	kg
Rolling inertia	I_{ex}	4000	kg·m^2
Nodding inertia	I_{ey}	6500	kg·m^2
Yawing inertia	I_{ez}	8500	kg·m^2
Longitudinal length	l_{ex}	5	m
Lateral length	l_{ey}	2.8	m
x-axis eccentric distance	x_e	0.6	m
y-axis eccentric distance	y_e	0.3	m

2.1 Connection scheme

According to research on arranging the hanging points of UCE, each hanging point needs to support the equipment equally. Therefore, a uniform and symmetrical distribution is usually adopted; that is, the same number of lifting points are evenly distributed on both sides of the symmetry axis of the equipment plane. A four-point connection is generally applied in conventional equipment, meaning that one hanging point is arranged on each of the four corners of the equipment, as shown in Fig. 1(a). Owing to the large size and mass of the equipment in this study, six-point and eight-point connection schemes are proposed, as shown in Fig. 1(b) and (c), respectively.

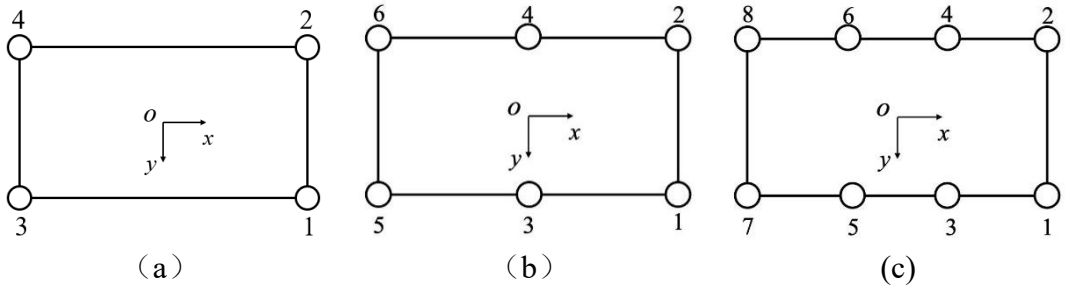

Fig. 1 Multi-point connection schemes of under-chassis equipment (UCE) (a) four-point; (b) six-point; (c) eight-point

Rigid and elastic connections comprise the two hanging methods for under-chassis equipment. Rigid connections are used for light and small equipment, whereas elastic connections are applied for large and heavy connections. According to the shape features, the lateral and longitudinal stiffness of a rubber component is usually related to the vertical stiffness value. In this study, wedge-

shaped rubber elements were used. The ratio of the lateral stiffness to the vertical stiffness was 1/3, and the longitudinal-vertical ratio was 1; these can be denoted, respectively, as follows:

$$\begin{cases} k_{yi} = k_{zi} / 3 \\ k_{xi} = k_{zi} \end{cases} \tag{1}$$

In the above, k_{zi}, k_{yi}, *and* k_{xi} stand for the vertical, lateral, and longitudinal stiffness of the i-th rubber element, respectively.

2.2 Modelling of UCE

A four-point connection scheme was used as an example for the modelling and analysis of the UCE. To consider the coupling vibration of different degrees of freedom (DOF), the UCE was set as a spatial rigid body with 6-DOF, and the rubber element was set as a spring with three-dimensional stiffness. The coordinate system was established as shown in Fig. 2. The origin of the coordinates was the centre of gravity of the equipment. The driving direction of the vehicle was the positive *x*-direction, the right side was the positive *y*-direction, and the vertical downward direction was the positive *z*-direction. The positive directions for rolling (α), nodding (β), and yawing (γ) were determined using the right-hand rule.

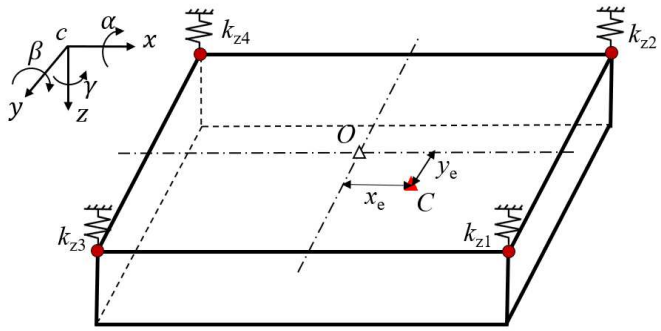

Fig. 2 Four-point connection scheme

The position coordinates of the *i*-th rubber element were set as (a_i,b_i,c_i), and the three-dimensional stiffness values were k_{xi}, k_{yi}, and k_{zi}, respectively. By using a matrix assembly method[12] to establish the dynamic equation for the UCE, the correlation matrix between the three-dimensional stiffness and 6-DOF of the i-th rubber element could be obtained as follows:

$$K_{tri} = \begin{bmatrix} -1 & 0 & 0 & 0 & -c_i & b_i \\ 0 & -1 & 0 & c_i & 0 & -a_i \\ 0 & 0 & -1 & -b_i & a_i & 0 \end{bmatrix} \tag{2}$$

By assembling the correlation matrix of all of the connection points, the correlation matrix of the suspension system between the stiffness and 6-DOF could be obtained as follows:

$$K_{tr} = \begin{bmatrix} K_{tr1} \\ \vdots \\ K_{trn} \end{bmatrix} \tag{3}$$

Then, the stiffness matrix of the suspension system could be acquired as follows:

$$K = K_{tr}' \cdot K_{ii} \cdot K_{tr} \tag{4}$$

In the above, K_{ii} represents the diagonal stiffness matrix, which comprises the three-dimensional

stiffness of all of the connection points.

The damping ratio of the rubber element was low, and had little effect on the coupling vibration. Therefore, the influence of the damping ratio was ignored in the decoupling degree analysis and modelling. The dynamic differential equation for the 6-DOF vibration of the equipment was obtained as follows:

$$M\ddot{X} + KX = 0 \tag{5}$$

Here, M is the mass matrix, which is composed of the mass and inertia of the equipment. X represents the status of the equipment. It can be verified that the dynamic differential equations obtained by the six-point and eight-point schemes are similar to Eq. (5).

2.3 Static analysis

A static force analysis was performed for the suspension system of the UCE. For each hanging point, the static balance equation of the rubber was obtained according to Hooke's law, as follows:

$$F_i = k_{zi} \cdot \delta_i \tag{6}$$

In the above, F_i is the reaction force of the i-th rubber, k_{zi} is the vertical stiffness of the i-th rubber, and δ_i is the static deflection of the i-th rubber; the latter was determined based on the vertical displacement (z), rolling angle (α), and nodding angle (β) of the equipment, as follows:

$$\delta_i = z + b_i \cdot \alpha + a_i \cdot \beta \tag{7}$$

When the equipment is in a static equilibrium position, the vertical force is balanced. The weight of the equipment is equal to the reaction force provided by the rubber elements, and the torques of the x -and y-axes are balanced. Then, the static balance equation of the UCE could be expressed as follows:

$$\begin{cases} \sum_{i=1}^{n} F_i = mg \\ \sum_{i=1}^{n} F_i \cdot a_i = 0 \\ \sum_{i=1}^{n} F_i \cdot b_i = 0 \end{cases} \tag{8}$$

The ratio of the dynamic stiffness to the static stiffness of the rubber elements commonly used in UCE suspension systems is between 1.0 and 3.5, and was selected as 1.5 in this study. The dynamic stiffness of the equipment depended on the mass of the equipment, natural frequency, and number of hanging points, as follows:

$$\sum_{i=1}^{n} k_{zi} = M_{\mathrm{e}} \left(\frac{f_{\mathrm{d}}}{2\pi} \right)^2 / q \tag{9}$$

Here, M_{e} is the mass of the equipment, f_{d} is the vertical natural frequency, and q is the number of hanging points.

The optimal vertical natural frequency was set as 9.55 Hz, as discussed Section 4.3. Based on Eq. (6) to Eq. (9), the static deflection and support reaction force of the multipoint connection method were calculated, as shown in Fig. 3. In each connection method, the vertical stiffness values of each hanging point were equal. It can be seen from the figure that increasing the number of

hanging points was beneficial for reducing the static stiffness requirements and reaction forces of each hanging point.

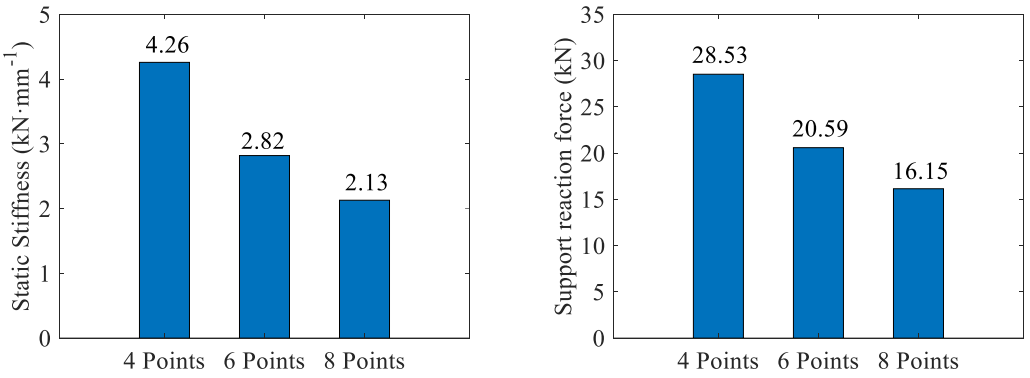

(a) Static stiffness (b) support reaction force

Fig. 3 Static stiffness and support reaction force

3 Optimal design of energy decoupling degree for UCE

3.1 Energy decoupling rate

The solution of the free vibration of the UCE was set to $X = Ae^{i\omega t}$. Rearranging Eq. (5) resulted in a calculation as follows:

$$\left(K - \omega^2 M\right) Ae^{i\omega t} = 0 \tag{10}$$

In the above, A is the amplitude of the displacement.

By assuming $\left|K - \omega^2 M\right| = 0$, the p-th (p = 1,2…6) vibration mode frequency ω_p and corresponding mode vector A^p were acquired.

In general, a mode vector analysis can be used to determine that coupling vibration exists in the different DOFs of equipment. The mode vector can reflect the proportional relationship of the vibration amplitude of each DOF at a specific frequency, and the kinetic energy contribution of each DOF under the main vibration shape can be calculated. The vibration kinetic energy of the j-th element in the i-th mode vector is defined as follows[13]:

$$E_{pj} = \frac{1}{2} M_{jj} \cdot \left(\Phi_{pj}\right)^2 \cdot \left(\omega_p\right)^2 \tag{11}$$

Here, M_{jj} is the value in the mass matrix, Φ_{pj} is the j-th element in the p-th mode vector, and ω_p is the natural frequency of the p-th mode vector.

The coupling degree of a multi-DOF system reflects the degree of mutual influence of the vibration between the respective DOFs. It can be expressed as the ratio of the maximum kinetic energy of the p-th DOF in the j-th main vibration mode to the total kinetic energy. Therefore, the energy decoupling degree can be defined as follows:

$$KE_{pj} = \frac{E_{pj}}{E_p} = \frac{M_{jj} \cdot \left(\Phi_{pj}\right)^2 \cdot \left(\omega_p\right)^2}{\sum_{j=1}^{6} M_{jj} \left(\Phi_{pj}\right)^2 \cdot \left(\omega_p\right)^2} \tag{12}$$

If KE_{pj} =100%, the energy of the j-th order vibration mode is concentrated in the p-th element, that is, the vibration of the j-th order vibration mode of the UCE is completely decoupled. Hence, the matrix KE can be used to describe the dynamic features of the system.

3.2 Optimisation method of energy decoupling degree

The decoupling optimisation objective of the UCE consisted of two parts: the energy decoupling degree of the system should be as high as possible, and the vertical natural vibration frequency of the UCE should coincide with the design frequency. The first part aimed to ensure that the vibrations between the different DOFs of the system did not affect each other, and the second aimed to make the equipment act as the DVA of the carbody, so as to achieve the vibration suppression effect. The obtained energy decoupling degree optimisation design objective function was as follows:

$$\begin{aligned} \min \ \ & g(x) = \sum_{p=1}^{6} \sigma_p \left[1 - \max KE(p, j)\right]^2 + \sum_{j=1}^{6} \kappa_j \left(\frac{f_0(j) - f(j)}{f_0(j)} \right)^2 \\ s.t. \ & \begin{cases} k_{\mathrm{L}} \le k_{zi} \le k_{\mathrm{U}} \\ k_{yi} = k_{zi} / 3, k_{xi} = k_{zi} \end{cases} \end{aligned} \tag{13}$$

In the above equation, σ_p represents the energy decoupling degree weight coefficients for each DOF, where the vertical weight is set to 1, and the rest are set to 0.5. κ_j is the weight coefficient of the difference between the natural frequency and design frequency. As the vertical natural frequency had a significant impact on the vibration of the carbody, only the vertical natural frequency was weighted here; that is, when the degree of freedom corresponding to j was vertical, κ_j was taken as 1, and the rest were taken as 0. k_{L} and k_{U} are the upper and lower limits of the allowable range for the production/installation of the rubber element stiffness, respectively. Eq. (13) was solved using an applicable genetic algorithm with a strong ability for global optimisation[14].

4 Rigid-flexible coupling dynamic model of a high-speed electric multiple-unit (EMU) train

4.1 Establishment and modal analysis of vehicle finite element model

Generally, the vibration of a carbody is formed by the superposition of the rigid and elastic vibrations. Some previous studies only defined the carbody as a rigid body, which resulted in the simulation results omitting the elastic vibration part. Instead, the carbody should be regarded as a flexible system with local dynamic deformations. The rigid-flexible coupling model considers the coupling of the self-deformations of the flexible body and vibrations of the system. This can make the simulation test more closely resemble a real situation.

In this study, a finite element model of the carbody was used to establish the elastic carbody for the rigid-flexible coupling dynamic model. Herein, the shell unit (shell 181, mesh size 40 mm) discretion of the entity model of the carbody was achieved by using a finite element analysis to obtain a finite element model of the carbody with 256485 nodes and 365453 units. The material

used was an aluminium alloy. The density of the material was 2700 kg/m^3, and the elastic constant was 69 GPa. Using model analysis, the low-order modal information of the carbody was acquired. Fig. 4 shows the eigenfrequency results for the first five orders of the carbody. As observed, the diagonal distortion modal frequency of the carbody was below 10 Hz, which worked against the ride quality. The first-order vertical bending frequency was 11.94 Hz; this was used as the basis for the design of the vertical natural frequency of the equipment suspension.

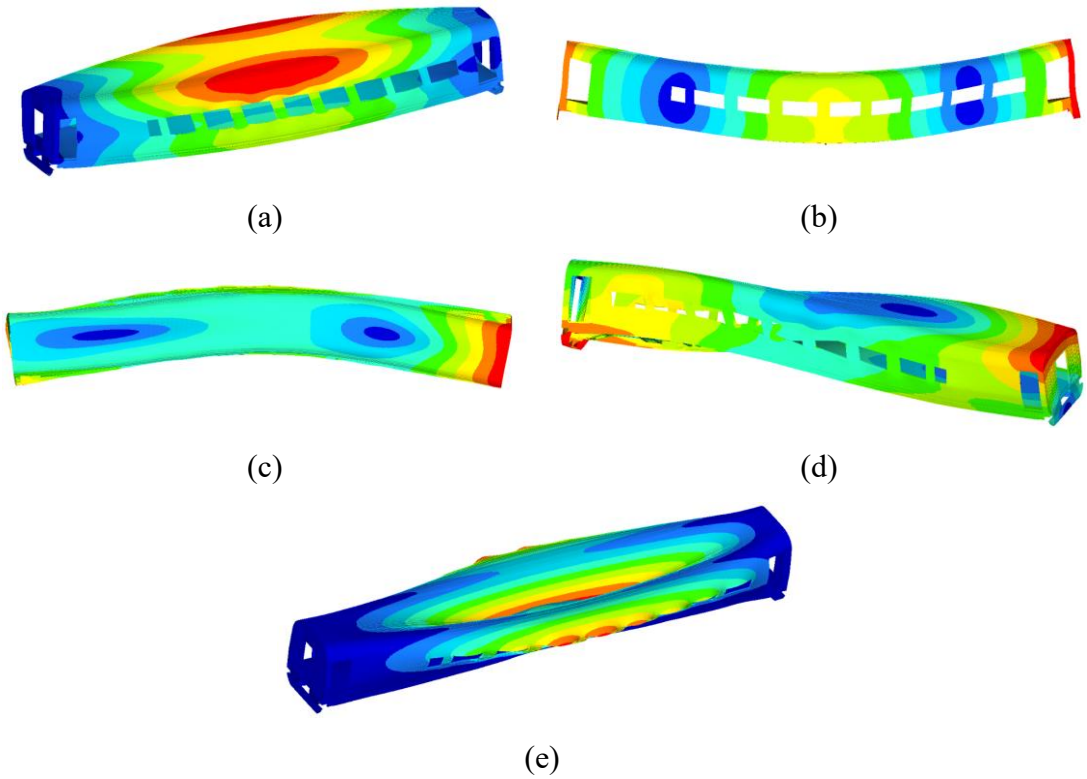

Fig. 4 Eigenfrequency results of the first five orders of the carbody: (a) diamond-shaped deformation mode at 9.68 Hz; (b) first-order vertical bending mode at 11.94 Hz; (c) first-order lateral bending mode at 12.49 Hz; (d) first-order torsional mode at 14.33 Hz; (e) breathing mode at 15.63 Hz

4.2 Establishment of rigid-flexible coupling dynamic model

By employing the multi-body dynamic simulation software SIMPACK, a rigid-flexible coupling dynamic model for the high-speed train was established, as shown in Fig. 5. In the model, the elastic carbody was obtained based on a condensation calculation[15]; this approach is commonly used to reduce the number of DOFs of an elastic carbody, and to obtain a model file containing the carbody structure and modal information. The model file was then imported into the dynamic model via the FEMBS interface of SIMPACK. According to the contribution of the carbody elasticity to vibration energy[16], only the main low-order elastic modes in Fig. 4 needed to be considered. The rest of the model was considered as rigid, including two bogies, eight axle boxes, four wheelsets, and one piece of equipment. In addition, the rigid-flexible model also considered the increasing stiffness of the secondary lateral elastic bump stop, nonlinearity of the wheel-rail contact, nonlinear creep force, creep torque, and nonlinearity of the hydraulic vibration absorber. The dynamic parameters are listed in Table A1 in the Appendix.

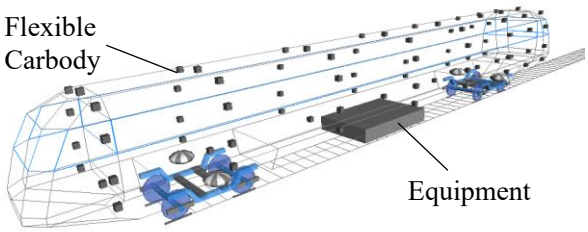

Fig. 5 Rigid-flexible coupling dynamic model

A high-speed track irregularity[17] was adopted in the model; the lateral and vertical irregularity waves are shown in Fig. 6.

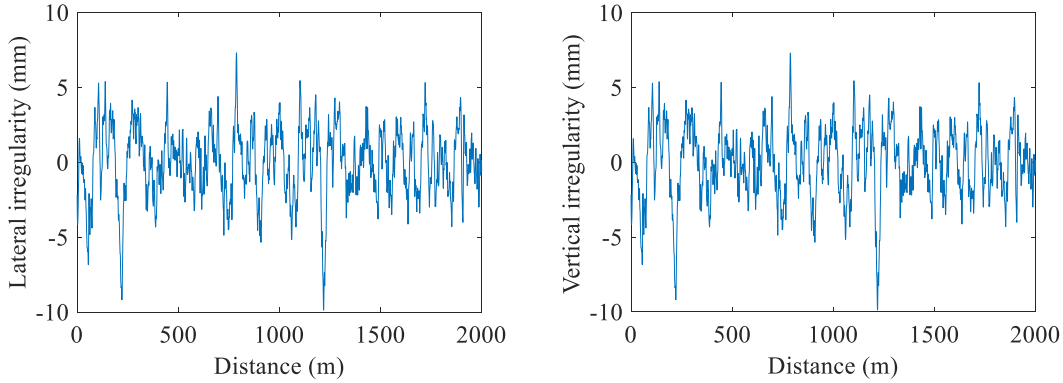

(a) (b)

Fig. 6 Track irregularity waves: (a) lateral irregularity; (b) vertical irregularity

4.3 Optimisation design of hanging frequency of the UCE based on dynamic vibration absorber (DVA) theory

In general, the vehicle is excited by the track irregularities while running, and the movements of the carbody and equipment will affect each other. A common method for hanging equipment is to design the UCE as a DVA of the carbody, aiming to suppress the first-order vertical bending vibration[18]. A DVA generally comprises an auxiliary mass, spring, and damping. Its working principle is based on using the anti-resonance characteristics of a multi-DOF system. When the main system vibrates, the DVA attached to it vibrates. Owing to the dynamic action of the absorber, the force acting on the main system by the absorber is in the opposite direction of the external exciting force, but with a similar amplitude. The forces acting on the main system counteract each other, such that the vibration of the main system is reduced. Fig. 7 shows a typical model of a DVA, where $m1$ and $k1$ are the mass and stiffness of the main system, respectively; $m2$, $k2$, and $c2$ are the mass, stiffness, and damping of the absorber, respectively.

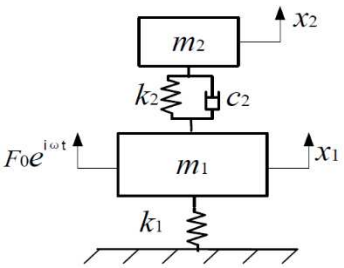

Fig. 7 Typical model of a dynamic vibration absorber

Assuming that the main system is affected by a harmonic excitation, the vibration dynamic

equation of the main system and absorber can be expressed as follows:

$$\begin{cases} m_1\ddot{x}_1 + k_1x_1 + c_2(\dot{x}_1 - \dot{x}_2) + k_2(x_1 - x_2) = F_0e^{i\omega t} \\ m_2\ddot{x}_2 - k_2\left(x_1 - x_2\right) - c_2\left(\dot{x}_1 - \dot{x}_2\right) = 0 \end{cases} \tag{14}$$

The responses of the main system and the absorber can be expressed as $x_1 = X_1e^{i\omega t}$, $x_2 = X_2e^{i\omega t}$, respectively. Then, the acceleration of the main system is as follows:

$$\ddot{x}_1 = -\omega^2 X_1e^{i\omega t} = \bar{A}_1e^{i\omega t} \tag{15}$$

In the above, $\bar{A}_1$ is the complex amplitude of the acceleration. The vibration amplitude ratio $\bar{A}_1 / F_0$ can be obtained as follows:

$$\frac{\bar{A}_1}{F_0}(\omega) = \frac{-\omega^2\left(m_2\omega^2 + k_2 + i\omega c_2\right)}{\left(-m_1\omega^2 + k_1\right)\left(-m_2\omega^2 + k_2\right) - m_2k_2\omega^2 + i\omega c_2\left(-m_1\omega^2 + k_1 - m_2\omega^2\right)} \tag{16}$$

Both the numerator and denominator in the above equation are divided by $(m_1m_2)^2$, and the following parameters are imported: the static deflection of the main system under a static force F_0 $X_{st} = F_0/k_1$, mass ratio of the absorber and main system $\mu = m_2/m_1$, natural frequency ratio of the absorber and the main system $\gamma = \sqrt{k_2/m_2}\Big/\sqrt{k_1/m_1}$, damping ratio of the absorber $\zeta = c_2/2\sqrt{m_2k_2}$, and ratio of the external excitation frequency to the natural frequency of the main system $\lambda = \omega\Big/\sqrt{k_1/m_1}$. Then, Eq. (16) can be simplified to the form of the real amplitude ratio, as follows:

$$\frac{A_1}{X_{st}}(\omega) = \sqrt{\frac{\left(\lambda^2\right)^2\left[\left(\gamma^2 - \lambda^2\right)^2 + \left(2\zeta\lambda\right)^2\right]}{\left[\left(1-\lambda^2\right)\left(\gamma^2 - \lambda^2\right) - \mu\gamma^2\lambda^2\right]^2 + \left[1 - \left(1+\mu\right)\lambda^2\right]^2\left(2\zeta\lambda\right)^2}} \tag{17}$$

According to the DVA theory and railway vehicle carbody vibration properties, the carbody and equipment can be simplified as a double-DOF system. In this study, the carbody was considered as the main system, and the equipment was considered as the absorber. To obtain the optimisation parameters for the DVA design, parameters were defined as follows:

$$f_e = \frac{1}{2\pi}\sqrt{\frac{k_e}{m_e}} \quad \mu = \frac{M_e}{M_c} \quad \eta = \frac{f_e}{f_c} \tag{18}$$

The first vertical bending frequency was defined as the natural frequency of the carbody, and made the greatest contribution to the vertical elastic vibration of the carbody. Using the fixed-point theory[18], the optimum frequency ratio of the natural frequency of the equipment and the carbody was considered as follows:

$$\eta_{opt} = \frac{1}{1+\mu} \tag{19}$$

Tab. 2 summarises the definitions and values of the parameters in Eqs. (18) and (19). The optimum frequency of the equipment if the vertical target frequency of the energy-decoupling degree optimisation design objective function shown in Eq. (13).

Tab. 2. Parameters of the dynamic vibration absorber system

Parameter	Symbol	Value	Unit
Mass of the equipment	M_e	8000	kg
Mass of the carbody	M_c	32000	kg
Natural frequency of the carbody	f_c	11.94	Hz
Mass ratio	μ	0.245	-
The optimum frequency ratio	η_{opt}	0.896	-
The optimum frequency of the equipment	f_e	9.55	Hz

5 Simulation experiment

Based on the decoupling optimisation objective function, a genetic algorithm was adopted to optimise the suspension stiffness of the four-point, six-point and eight-point connection schemes. Then, the optimisation results were input into the rigid-flexible coupling dynamics model for time-domain simulation experiments. The energy decoupling degree, vertical natural frequency of the equipment, ride quality of the carbody, acceleration frequency amplitude spectrum of the carbody, and dynamic reaction force of the rubber element were analysed.

Fig. 8 illustrates the decoupling degree of each degree before and after decoupling optimisation. DOFs 1–6 represent the motions of longitudinal (x), lateral (y), vertical (z), rolling (α), nodding (β), and yawing (γ), respectively. It can be seen from the figure that after the decoupling optimisation calculation, the decoupling degree of the three suspension schemes is improved to a certain extent, and all of the average decoupling degrees are more than 96%. Before decoupling optimisation, coupled vibrations exist in the translation and rotation motions in the x and z directions. After decoupling optimisation, the coupled vibrations are significantly reduced.

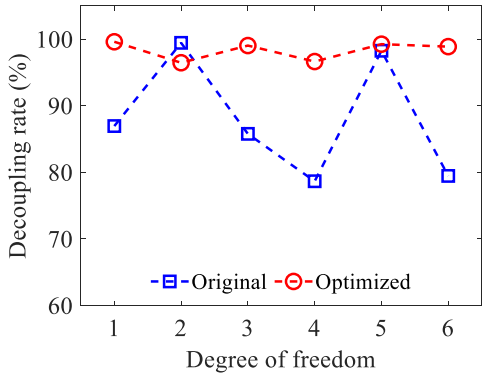

(a)

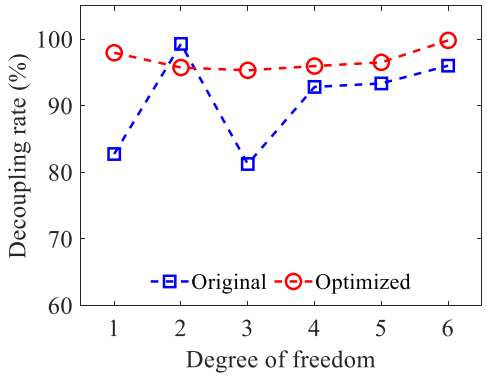

(b)

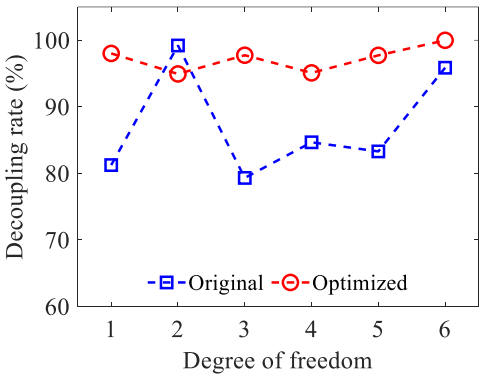

(c)

Fig. 8 Energy decoupling degree: (a) four-points; (b) six-point; (c) eight-point

Fig. 9 compares the vertical natural frequency of the equipment before and after decoupling optimisation. It can be seen from the figure that before decoupling optimisation, the vertical natural vibration frequency of the equipment with the different connection schemes is between 8.5 and 9 Hz. After decoupling optimisation, they are all approximately 9.55 Hz (the red dashed line in the figure); this beneficial to reducing the vibration of the equipment in the vertical direction, and for providing a DVA for the first-order vertical bending mode.

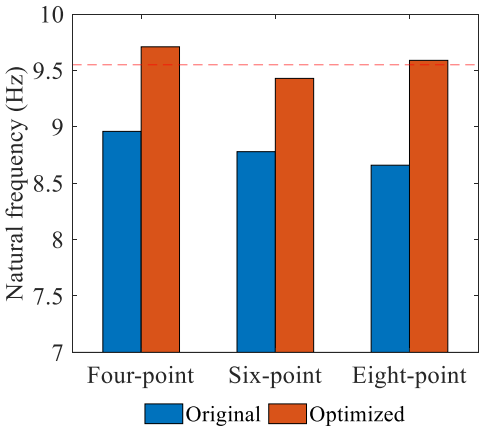

Fig. 9 Vertical natural frequency of the equipment

The Sperling index[19] is an index for evaluating the ride quality of railway vehicles. The lower the index value, the better the ride quality. Fig. 10 shows a comparison of the Sperling index of the carbody before and after decoupling optimisation. It can be seen that after decoupling optimisation, the lateral ride quality is improved to a certain extent when the speed exceeds 300 km/h, and the vertical ride quality is significantly improved at all speed levels. Decoupling optimisation decouples the vibrations between the different degrees of freedom of the UCE. The vertical vibration natural frequency of the equipment and natural frequency of the vehicle body are optimally synchronised to achieve the optimal vibration absorption effect. Therefore, the vibration of the carbody is reduced, and the running ride quality is improved. The comparative analysis of the different connection schemes shows that there is little difference in the ride quality between the different schemes before and after decoupling optimisation.

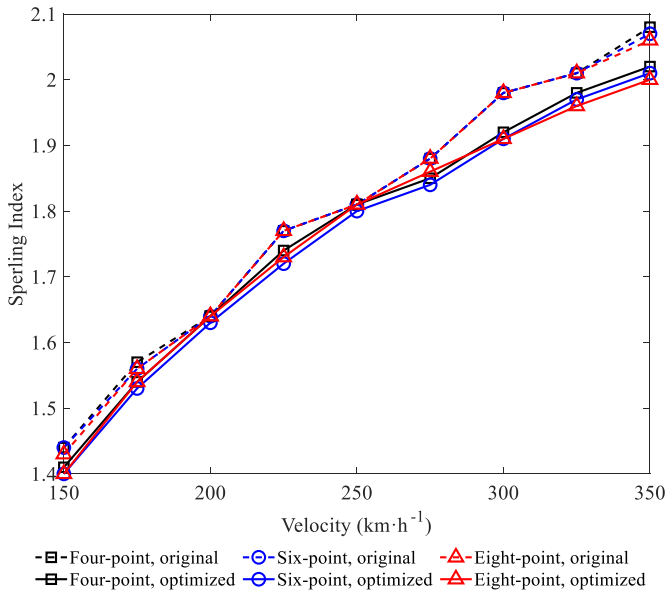

(a)Lateral

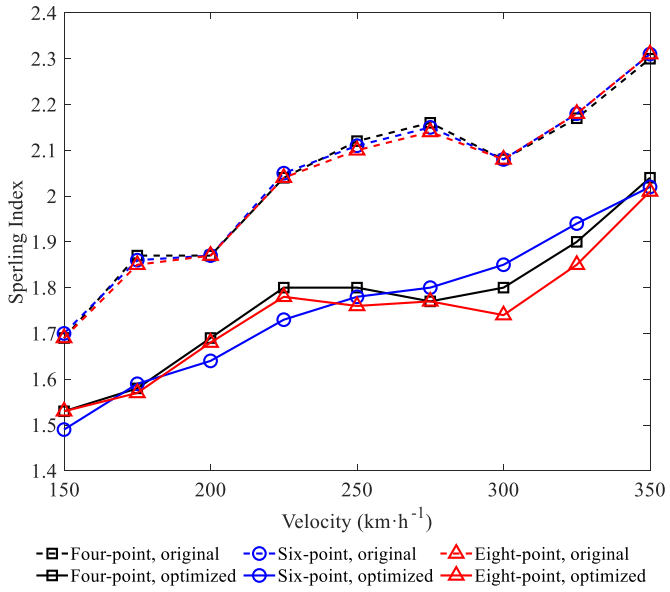

(b)Vertical

Fig. 10 Sperling index

The acceleration frequency amplitude spectra of the carbody at a speed of 350 km/h in the different connection schemes are shown in Fig. 11. After decoupling optimisation, the amplitude of the lateral vibration acceleration at 12–16 Hz is reduced to a certain extent, and the vertical vibration acceleration is significantly reduced at 10–15 Hz. This demonstrates that the vertical dynamic vibration absorption effect of the equipment is significantly improved by the decoupling optimisation. As a result, the vibration amplitude near the first-order vertical bending mode vibration frequency (11.94 Hz) of the carbody is significantly reduced.

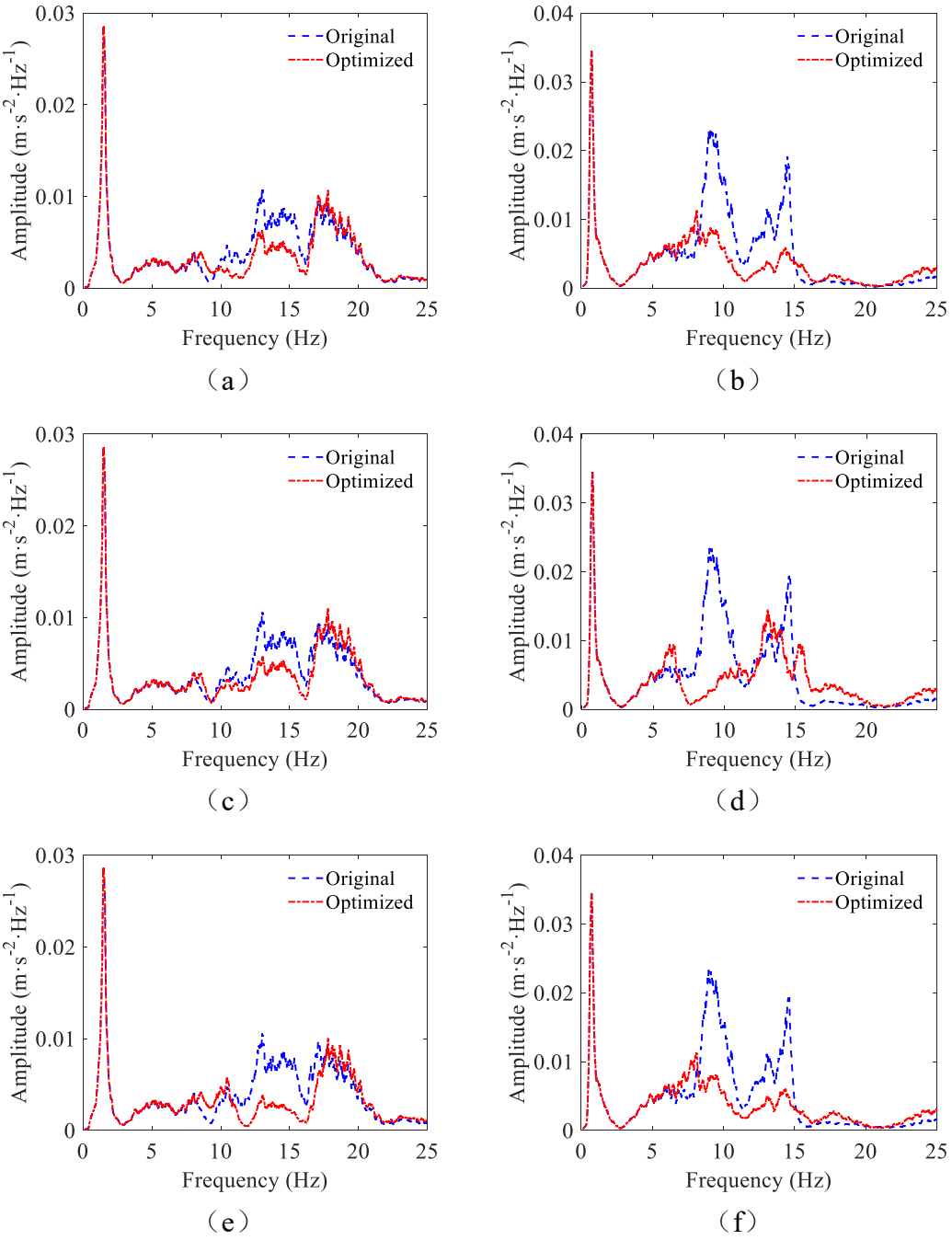

Fig. 11 Acceleration frequency amplitude spectrum of the carbody: (a) four-point, lateral; (b) four-point, vertical; (c) six-point, lateral; (d) six-point, vertical;(e) eight-point, lateral; (f) eight-point, vertical

The maximum dynamic reaction forces of the different connection schemes all appear at the No. 1 hanging point (see Fig. 1); this is caused by the eccentricity of the equipment toward the hanging point. The simulation results after the decoupling optimisation of the dynamic reaction forces at the No. 1 hanging point of the different connection schemes are shown in Fig. 12. It can be seen that the dynamic reaction force amplitude decreases significantly as the number of hanging points increases. The amplitude of the dynamic reaction force of the eight-point scheme is only half that of the four-point scheme.

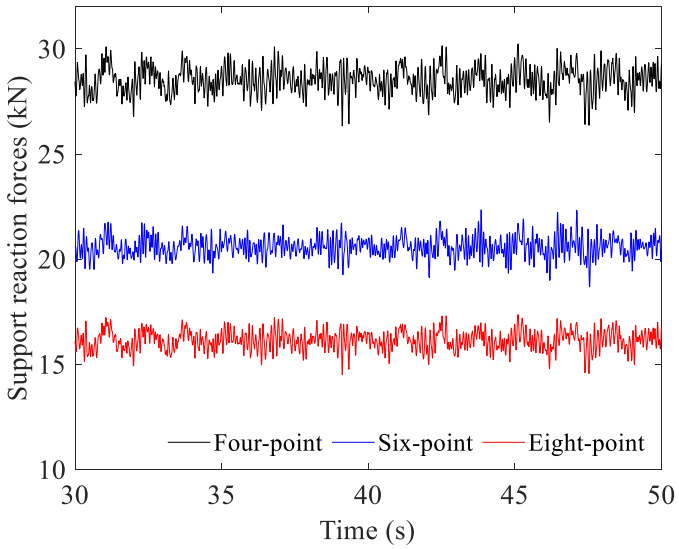

Fig. 12 Dynamic support reaction forces

6 Conclusions

This research proposed a multi-point connection method for heavy and large UCE based on the eccentricity of high-speed trains. The static deflection and supporting reaction force of the equipment with the multi-point connection method were studied based on a static analysis. The results showed that increasing the number of hanging points is beneficial for reducing the stiffness requirements of each rubber element. The dynamic vibration equation of the equipment was established, and the energy decoupling degree of the equipment was optimised using a genetic algorithm. The energy decoupling degree of the equipment significantly improved after the decoupling optimisation. A rigid-flexible coupling dynamic model of a high-speed EMU train was built to analyse the vibration and ride quality of the carbody with different multipoint suspension schemes. The results implied that after decoupling optimisation, the vibration amplitude of the carbody was effectively reduced, and the running ride quality of the carbody was improved. The difference in the number of hanging points had little effect on the vibration performance of the carbody. However, increasing the number of hanging points was beneficial for reducing the dynamic support reaction forces of the hanging points, which was beneficial for reducing the dynamic stress of the hanging components and improving the anti-fatigue performance.

Declarations

Availability of data and materials.

Acknowledgements

Not applicable.

Authors' contributions

Yu Sun was in charge of the whole research and wrote the manuscript; Jinsong Zhou discussed and read the manuscript; Dao Gong and Yuanjin Ji assisted with the analysis; Taiwen You and Jiangxue Chen assisted with data processing; Qiushi Wang and Tengfei Wang assisted with validation and figures. All authors read and approved the final manuscript.

Authors’ Information

Yu Sun, born in 1991, is currently a post doctor in Postdoctoral Station of Mechanical Engineering, Tongji University. He received his Ph.D in Vehicle Operation Engineering from Tongji University. His research interests include railway vehicle dynamics and vibration control.

Jinsong Zhou, born in 1969, is currently a Professor in Institute of Rail and Transit, Tongji University. He received his Ph.D in Mechanical Engineering from Shanghai Jiaotong Uni-versity. He has been researching on railway vehicle dy-namics, modal parameter testing and control of vibration and sound of railway vehicles.

Dao Gong, born in 1985, is currently an Associate Professor in Institute of Rail and Transit, Tongji University. He received his Ph.D in Vehicle Operation Engineering from Tongji University. He has been researching on railway vehicle vibration testing and control.

Yuanjin Ji, born in 1989, is currently a post doctor in Postdoctoral Station of Mechanical Engineering, Tongji University. He received his Ph.D in Vehicle Operation Engineering from Tongji University. His research focus on wheel-rail contact.

Taiwen You, born in 1992, is currently a Ph.D candidate in Vehicle Operation Engineering, Tongji University. His research focus on elastic vibration of rail vehicles.

Jiangxue Chen, born in 1994, is currently a Ph.D candidate in Vehicle Operation Engineering, Tongji University. His research focus on parameter identification of rail vehicles.

Qiushi Wang, born in 1991, is currently a Ph.D candidate in Vehicle Operation Engineering, Tongji University. His research focus on fatigue life assessment research.

Tengfei Wang, born in 1995, is currently a Ph.D candidate in Vehicle Operation Engineering, Tongji University. His research focus on wheel irregularity research.

Funding

This work is supported by National Natural Science Foundation of China (grant no. 51805373), Postdoctoral Innovation Talent Support Program (grant no. BX20200240), China Postdoctoral Science Foundation (grant no. 2020M671207).

Competing interests

No potential conflict of interest was reported by the authors.

References

[1] Sun Y, Zhou J, Gong D, et al. Vibration control of high-speed trains self-excitation under-chassis equipment by HSLDS vibration isolators. J Mech Sci Technol, 2019,33(1):65-76.

[2] Gong D, Zhou J, Sun W. Influence of under-chassis-suspended equipment on high-speed EMU trains and the design of suspension parameters. Proc Institution Mech Engineers Part F-J Rail Rapid Transit, 2016,230(8):1790-1802.

[3] Chen J, Wu Y, Zhang L, et al. Dynamic optimization design of the suspension parameters of car body-mounted equipment via analytical target cascading. J Mech Sci Technol, 2020,34(5):1957-1969.

[4] Wang Q, Zeng J, Wei L, et al. Carbody vibrations of high-speed train caused by dynamic unbalance of underframe suspended equipment. Adv Mech Eng, 2018,10(12):1-13.

[5] Gong D, Zhou J S, Sun W J. On the resonant vibration of a flexible railway car body and its suppression with a dynamic vibration absorber. J Vib Control, 2013,19(5):649-657.

[6] Sun Y, Gong D, Zhou J, et al. Low frequency vibration control of railway vehicles based on a high static low dynamic stiffness dynamic vibration absorber. Sci China Technol Sci, 2019,62(1):60-69.

[7] Sun Y, Zhou J, Gong D, et al. A New Vibration Absorber Design for Under-Chassis Device of a High-Speed Train. Shock Vib, 2017,2017:1-8.

[8] Shi H, Luo R, Wu P, et al. Application of DVA theory in vibration reduction of carbody with suspended equipment for high-speed EMU. Sci China Technol Sci, 2014,57(7):1425-1438.

[9] Huang C, Zeng J, Luo G, et al. Numerical and experimental studies on the car body flexible vibration reduction due to the effect of car body-mounted equipment. Proc Institution Mech Engineers Part F-J Rail Rapid Transit, 2018,232(1):103-120.

[10] Gong D, Zhou J, Sun W, et al. Method of multi-mode vibration control for the carbody of high-speed electric multiple unit trains. J sound Vib, 2017,409:94-111.

[11] Xia Z, Gong D, Zhou J, et al. Decoupling Optimization Design of Under-Chassis Equipment Suspension System in High-Speed Trains. Shock Vib, 2018,2018:6292595.

[12] Mao X. Research on Rail Grinding Profile Design Based on Wheel Rail Contact Characteristics. Shanghai: Tongji University, 2018.

[13] Sun B, Zhang Q, Sun Q, et al. Study on decoupled engine mounting system. J Vib Eng, 1994,3(7):240-245.

[14] Goldenberg D E. Genetic algorithms in search, optimization and machine learning. Boston, USA: Addison Wesley, 1989.

[15] Guyan R J, Reduction of stiffness and mass matrices, AIAA Journal, 1965,3(2): 1133–1145.

[16] Carlbom P F. Combining MBS with FEM for Rail Vehicle Dynamics Analysis. Multibody Syst Dyn, 2001,6(3):291-300.

[17] Zhou J. Vibration and Control on Railway Vehicles. Shanghai: Fudan University Press, 2020.

[18] Seto K. Dynamic Vibratin Absorber and its Applications. Beijin: China: Machine Press, 2013.

[19] Deng C, Zhou J, Thompson D, et al. Analysis of the consistency of the Sperling index for rail

vehicles based on different algorithms. Vehicle Syst Dyn, 2021,59(2):313-330.

Appendix

Table A1.

Parameters for the high-speed train dynamic model.

Symbols	Meanings	Values	Units
M_c	Carbody mass	38 000	kg
J_{cx}	Carbody rolling inertia	1.2×10^5	kg·m^2
J_{cy}	Carbody pitching inertia	1.65×10^6	kg·m^2
J_{cz}	Carbody yawing inertia	1.6×10^6	kg·m^2
m_f	Frame mass	2 900	kg
J_{fx}	Frame rolling inertia	1 240	kg·m^2
J_{fy}	Frame pitching inertia	2 230	kg·m^2
J_{fz}	Frame yawing inertia	3 340	kg·m^2
m_w	Wheelset mass	1820	kg
J_{wz}	Wheelset yawing inertia	700	kg·m^2
k_{px}	Longitudinal stiffness of primary suspension	1.2×10^7	kN/m
k_{py}	Lateral stiffness of primary suspension	4.9×10^6	kN/m
k_{pz}	Vertical stiffness of primary suspension	1×10^6	kN/m
c_{pz}	Vertical damping of primary suspension	10 000	N·s/m
k_{sx}	Longitudinal stiffness of secondary suspension	160	kN/m
c_{sx}	Longitudinal damping of secondary suspension	70 000	N·s/m
k_{sy}	Lateral stiffness of secondary suspension	160	kN/m
c_{sy}	Lateral damping of secondary suspension	5000	N·s/m
k_{sz}	Vertical stiffness of secondary suspension	220	kN/m
c_{sz}	Vertical damping of secondary suspension	10 000	N·s/m
h_{df}	Half of bogie distance	8.75	m
h_{da}	Half of axle distance	1.25	m
h_{dp}	Half of primary suspension lateral distance	1	m
h_{ds}	Half of secondary suspension lateral distance	0.95	m
r_0	Radius wheel	0.46	m